SCIENTIFIC REPORTS

OPEN

Two novel, putative mechanisms of action for citalopram-induced platelet inhibition

Received: 10 July 2018
Accepted: 12 October 2018
Published online: 12 November 2018

Harvey G. Roweth[1], Aaron A. Cook[2], Masaaki Moroi[3], Arkadiusz M. Bonna[3], Stephanie M. Jung[3], Wolfgang Bergmeier[2], Stewart O. Sage[1] & Gavin E. Jarvis[1]

Citalopram, a selective serotonin reuptake inhibitor (SSRI), inhibits platelet function *in vitro*. We have previously shown that this action is independent of citalopram's ability to block serotonin uptake by the serotonin transporter and must therefore be mediated via distinct pharmacological mechanisms. We now report evidence for two novel and putative mechanisms of citalopram-induced platelet inhibition. Firstly, in platelets, citalopram blocked U46619-induced Rap1 activation and subsequent platelet aggregation, but failed to inhibit U46619-induced increases in cytosolic Ca^{2+}. Similarly, in neutrophils, citalopram inhibited Rap1 activation and downstream functions but failed to block PAF-induced Ca^{2+} mobilisation. In a cell-free system, citalopram also reduced CalDAG-GEFI-mediated nucleotide exchange on Rap1B. Secondly, the binding of anti-GPVI antibodies to resting platelets was inhibited by citalopram. Furthermore, citalopram-induced inhibition of GPVI-mediated platelet aggregation was instantaneous, reversible and displayed competitive characteristics, suggesting that these effects were not caused by a reduction in GPVI surface expression, but by simple competitive binding. In conclusion, we propose two novel, putative and distinct inhibitory mechanisms of action for citalopram: (1) inhibition of CalDAG-GEFI/Rap1 signalling, and (2) competitive antagonism of GPVI in platelets. These findings may aid in the development of novel inhibitors of CalDAG-GEFI/Rap1-dependent nucleotide exchange and novel GPVI antagonists.

Citalopram, a selective serotonin reuptake inhibitor (SSRI), is widely used as an antidepressant[1]. Its primary pharmacological target is the serotonin transporter (SERT)[2,3] inhibition of which prevents cellular uptake of serotonin (5-hydroxytryptamine, 5-HT)[4]. SSRIs are widely believed to exert psychiatric benefit by inhibiting SERT and modifying serotonergic neurotransmission in the central nervous system[5]. SERT is also found on non-neuronal cells, including platelets, which store 5-HT in dense granules that resemble neurotransmitter vesicles[6,7]. Citalopram not only inhibits platelet SERT, but also platelet aggregation, adhesion, thromboxane A_2 (TxA_2) synthesis and dense granule release[8–12]. However, this functional inhibition is not caused by blockade of 5-HT uptake and must therefore be mediated by distinct pharmacological mechanisms of action[10].

Citalopram inhibits platelet aggregation induced by both collagen and the TxA_2 mimetic, U46619, countering the claim that it is a specific inhibitor of collagen-induced platelet activation[9]. Nevertheless, citalopram is a more potent inhibitor of collagen[10], which activates platelets predominantly via glycoprotein VI (GPVI), than U46619, a thromboxane prostanoid (TP) receptor agonist, suggesting differential mechanisms of action. Reduced phosphorylation of signalling proteins in the GPVI pathway[10] points to GPVI as a possible site of action for citalopram, which could act as a classical competitive antagonist or allosteric inhibitor. For example, citalopram could disrupt GPVI dimers that mediate collagen binding and platelet activation[13]. However, GPVI inhibition would not account for citalopram's effect on U46619-induced responses.

Both GPVI and TP receptor activation raise cytosolic calcium concentrations ($[Ca^{2+}]_{cyt}$), a shared signalling pathway for collagen, TxA_2, and many other platelet agonists. Although there are numerous reports of citalopram inhibiting platelet aggregation *in vitro*[8–12] few have directly measured its effect on Ca^{2+} signalling. Tseng *et al.*[14] reported that citalopram did not inhibit ADP-induced Ca^{2+} signalling, suggesting some specificity in the action of citalopram, perhaps downstream of increased $[Ca^{2+}]_{cyt}$. Elevated $[Ca^{2+}]_{cyt}$ upregulates GTP binding

[1]Department of Physiology, Development and Neuroscience, University of Cambridge, Cambridge, UK. [2]Department of Biochemistry and Biophysics, University of North Carolina at Chapel Hill, Chapel Hill, USA. [3]Department of Biochemistry, University of Cambridge, Cambridge, UK. Correspondence and requests for materials should be addressed to G.E.J. (email: gej1000@cam.ac.uk)

to the small GTPase Rap1, a process catalysed by the calcium and diacylglycerol guanine nucleotide exchange factor-1 (CalDAG-GEFI, also known as RAS guanyl-releasing protein 2)[15–17]. Rap1-GTP mediates the transition of integrin $\alpha_{IIb}\beta_3$ (also known as glycoprotein (GP) IIb/IIIa) to a high-affinity state, thereby facilitating platelet aggregation through fibrinogen crosslinks[18,19].

Therefore, our search for novel mechanisms for citalopram focussed on GPVI and Ca^{2+} signalling. We utilised the selective GPVI agonist, collagen-related peptide (CRP), and also investigated Ca^{2+} signalling in neutrophils, which share similar Ca^{2+}-dependent mechanisms of activation[20,21] and are also inhibited by SSRIs *in vitro*[22]. Our data reveal two novel, putative inhibitory mechanisms of action for citalopram.

Results

MECHANISM 1: Inhibition of CalDAG-GEFI-dependent Rap1 nucleotide exchange. *Differential inhibition of GPVI-dependent and U46619-induced calcium mobilisation.* Citalopram inhibits both collagen- and U46619-induced platelet aggregation[10]. Since aggregation is dependent on Ca^{2+} signalling, the effect of citalopram on agonist-induced increases in $[Ca^{2+}]_{cyt}$ was investigated. Cross-linked CRP (CRPXL), a selective agonist for GPVI, was used instead of collagen to generate exclusively GPVI-dependent responses. $[Ca^{2+}]_{cyt}$ was monitored in platelets pre-treated for approximately 5 min with citalopram (0, 10, 20, 50, 100 & 200 µM), before stimulation with either CRPXL (0.5 µg mL^{-1}) or U46619 (0.2 µM). These just sub-maximal concentrations of CRPXL and U46619 were selected based on prior pilot experiments (Supplementary Fig. S1).

CRPXL-induced increases in $[Ca^{2+}]_{cyt}$ were abolished by citalopram (Fig. 1a,b). The inhibitory potency of citalopram ($pIC_{50} = 4.34 \pm 0.09$ (N = 7 blood donors)) matched its potency for inhibiting collagen-induced aggregation ($pIC_{50} = 4.31 \pm 0.21$[10]). This is also consistent with our previous observations that citalopram inhibited tyrosine phosphorylation signalling downstream of GPVI[10]. Surprisingly, and in stark contrast, citalopram had no discernible effect on U46619-induced increases in $[Ca^{2+}]_{cyt}$ (Fig. 1c,d) (N = 7 blood donors).

To confirm that Fura-2-loading had no functional effect on platelets, on one occasion, U46619-induced aggregation was measured in the same preparation of Fura-2-loaded platelets used for Ca^{2+} measurements. Fura-2-loaded platelets aggregated normally in response to 0.2 µM U46619 (Fig. 1e) and citalopram (200 µM) inhibited this response, as expected. However, as reported above, the increase in $[Ca^{2+}]_{cyt}$ was unaffected by citalopram.

Thus, in citalopram-treated platelets, U46619 induced a normal Ca^{2+} response, but no aggregation, suggesting that citalopram inhibits aggregation at a point downstream of Ca^{2+} mobilisation. This conclusion was supported by the observation that citalopram also inhibited platelet aggregation induced by the Ca^{2+} ionophore, ionomycin (0.5 µM), in a concentration-dependent manner: $pIC_{50} = 3.98 \pm 0.09$ (N = 4 blood donors) (Supplementary Fig. S2).

Citalopram inhibits Rap1 activation in platelets. U46619-induced platelet activation was inhibited by citalopram, despite preserved Ca^{2+} store release (Fig. 1). We therefore aimed to identify where citalopram exerts its inhibitory effects downstream of Ca^{2+} release.

Increased $[Ca^{2+}]_{cyt}$ causes CalDAG-GEFI-mediated Rap1 activation and downstream platelet aggregation[15,17]. Experiments were conducted to determine if citalopram inhibits U46619-induced platelet aggregation by preventing Rap1 activation. The effect of citalopram (200 µM) on Rap1 activation induced by CRPXL (0.5 µg mL^{-1}) or U46619 (0.2 µM) was investigated. Activated Rap1 (Rap1-GTP) was isolated and quantified by Western blot analysis. The results (Fig. 2a) clearly show that citalopram inhibited both CRPXL- and U46619-induced Rap1-GTP formation ($P = 7.5 \times 10^{-9}$, F = 83.4, as determined by regression analysis (Supplementary Analysis 1)). Thus, Rap1 activation is blocked by concentrations of citalopram that inhibit U46619-induced platelet aggregation, but have no effect on Ca^{2+} release from intracellular stores.

Further experiments were conducted to investigate whether citalopram suppresses CalDAG-GEFI-mediated nucleotide exchange of isolated Rap1, using purified recombinant CalDAG-GEFI and Rap1B, the predominant Rap1 isotype in platelets[17,23]. Nucleotide exchange was monitored by detecting fluorescent BODIPY-FL-conjugated GDP as described in the Methods. Citalopram inhibited CalDAG-GEFI-mediated BODIPY-FL-GDP exchange onto Rap1B in a concentration-dependent manner (Fig. 2b,c). Peak increases in fluorescence intensity (ΔF.I.) were fitted to the four-parameter logistic (4PL) model, with the *Max* parameter constrained to the basal response, indicated by the ΔF.I. observed when no CalDAG-GEFI was added. The pIC_{50} value was 3.67 ± 0.32 (N = 4 experiments).

Citalopram inhibits Rap1 activation in neutrophils. The results above indicate that citalopram inhibits CalDAG-GEFI-dependent Rap1B nucleotide exchange and imply that other cells expressing CalDAG-GEFI/Rap1 would also be inhibited by citalopram. Similarly to platelets, neutrophils express both CalDAG-GEFI and Rap1 (the predominant form is also Rap1B[24]), which mediate agonist and Ca^{2+}-dependent activation[21,25]. Signalling and functional studies were therefore conducted on isolated neutrophils to determine the effects of citalopram treatment.

Platelet-activating factor (PAF) is a potent activator of neutrophils. PAF-induced (1 µM) increases in the $[Ca^{2+}]_{cyt}$ were measured following a 5 min citalopram pre-treatment (0, 10, 20, 50, 100, 200 & 500 µM). As with platelets, citalopram did not affect PAF-induced increases in $[Ca^{2+}]_{cyt}$ in neutrophils (N = 6 blood donors) (Fig. 3a,b), whereas PAF-induced (1 µM) Rap1 activation was inhibited by citalopram (200 µM) (Fig. 3c). ($P = 5.9 \times 10^{-6}$, F = 38.7, as determined by regression analysis (Supplementary Analysis 2)).

Citalopram inhibits neutrophil function. Rap1 regulates the transition of $\alpha_M\beta_2$ integrin (Mac-1, CD11b/18) to a high-affinity binding state in macrophages[26]. $\alpha_M\beta_2$ is a cell surface adhesion receptor for fibrinogen[27] and CalDAG-GEFI-deficient neutrophils stimulated with PAF show impaired $\alpha_M\beta_2$-dependent adhesion to fibrinogen[21].

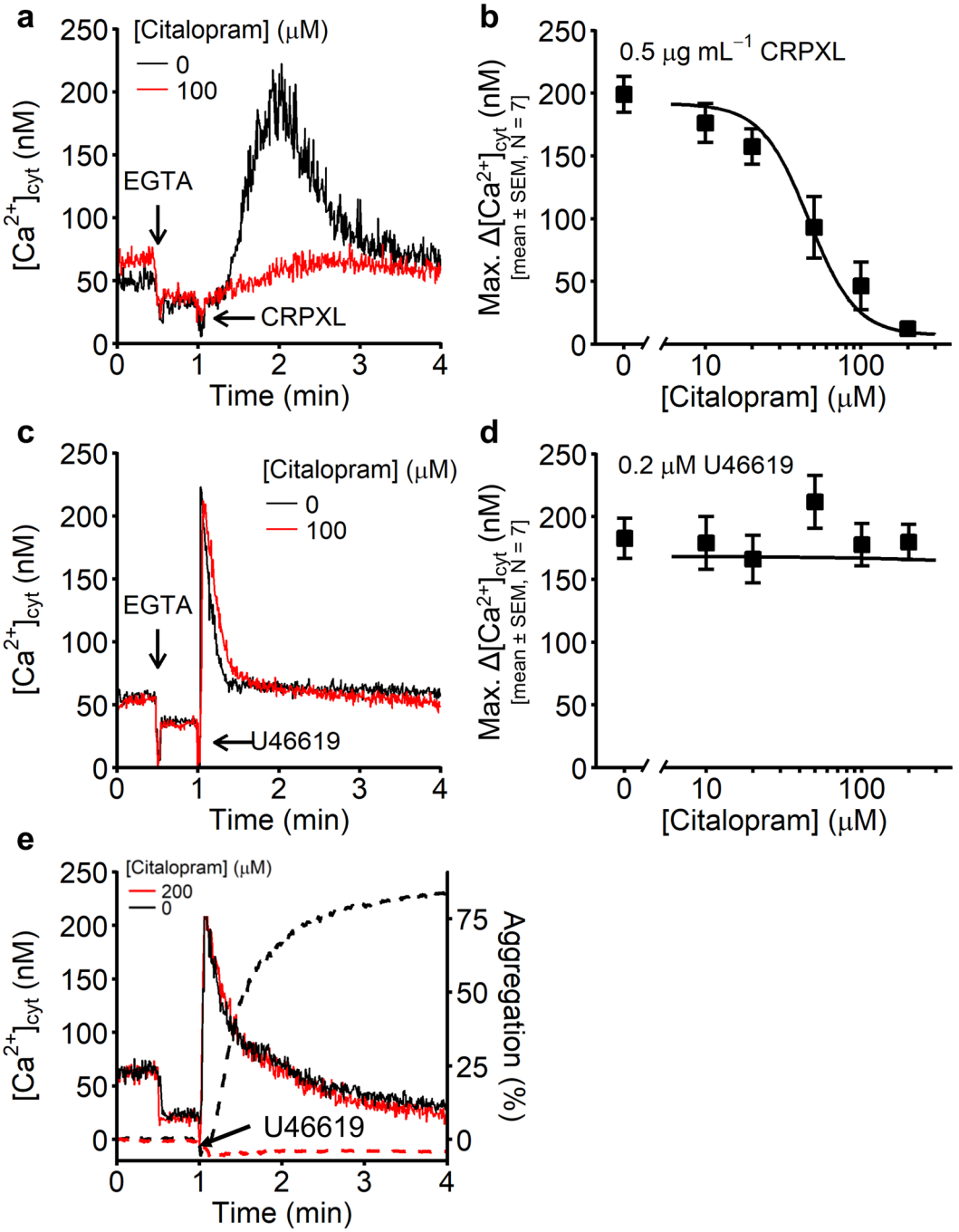

Figure 1. Calcium release from intracellular stores in either untreated or citalopram-treated platelets. Example traces are shown for both (**a**) cross-linked collagen-related peptide (CRPXL)-stimulated (0.5 μg mL^{-1}) and (**c**) U46619-stimulated (0.2 μM) platelets, either untreated or pre-treated with citalopram (100 μM) for approximately 5 min. (**b**,**d**) After the addition of agonist, the cytosolic concentration of Ca^{2+} ($[Ca^{2+}]_{cyt}$) in platelets pre-incubated with citalopram (0, 10, 20, 50, 100 & 200 μM) was recorded for 3 min. The maximum increase in $[Ca^{2+}]_{cyt}$ following agonist addition (Max. $\Delta[Ca^{2+}]_{cyt}$) was used to generate concentration-response curves, using the four-parameter logistic (4PL) model (N = 7 blood donors). (**e**) In a separate experiment, using platelets from the same blood donor on the same experimental day, $[Ca^{2+}]_{cyt}$ (solid lines) and aggregation (dashed line) were separately recorded following pre-incubation with or without citalopram (200 μM) and stimulation with U46619 (0.2 μM) (N = 1 blood donor).

Experiments were performed to determine if citalopram could inhibit activation of neutrophil integrin $\alpha_M\beta_2$. Neutrophils were pre-incubated with citalopram (0, 5, 10, 20, 50, 100, 200 & 500 μM) for approximately 5 min, followed by PAF stimulation (1 μM). Representative flow cytometry histograms show that citalopram inhibited

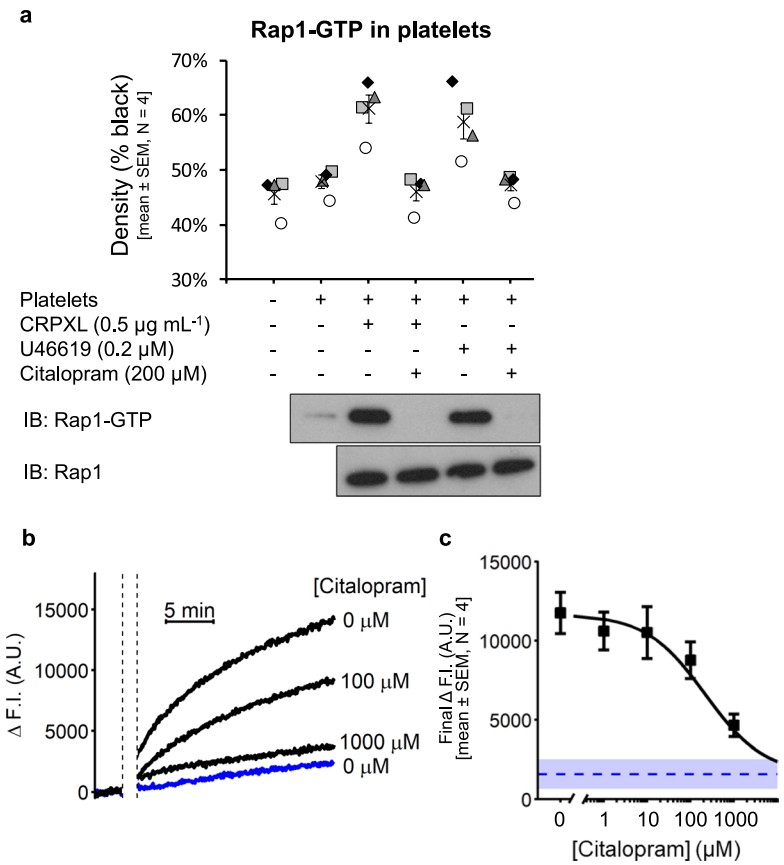

Figure 2. Citalopram inhibits Rap1-GTP formation in platelets. **(a)** Platelets were pre-treated with (+) or without (−) citalopram (200 µM) for approximately 5 min, before stimulation for 1 min with either cross-linked collagen-related peptide (CRPXL, 0.5 µg mL^{-1}) or U46619 (0.2 µM). Rap1-GTP was isolated from unstimulated and agonist-stimulated platelets and quantified using densitometry following SDS-PAGE and Western blotting. Total Rap1 levels were also measured. (N = 4 blood donors. Different donors are indicated by different symbols and the mean by ×). (**b**) Example traces from a BODIPY-FL-GDP fluorescence-based assay, which was used to monitor the nucleotide exchange activity of Rap1B. CalDAG-GEFI was pre-incubated with citalopram (0, 100 & 1000 µM) for approximately 5 min before its addition to wells (white segment, black dashed lines) containing BODIPY-FL-GDP and Rap1B. The blue trace indicates fluorescence in the absence of CalDAG-GEFI. (**c**) Following CalDAG-GEFI pre-incubations with citalopram (0, 1, 10, 100 & 1000 µM), the increase in fluorescence intensity 20 min after the addition of CalDAG-GEFI (Final ΔF.I.) was used to create concentration-response curves. The blue dashed line (mean), and blue area (±SEM) show the Final ΔF.I. in the absence of CalDAG-GEFI, which was used to constrain the *Max* parameter of the four-parameter logistic (4PL) model (N = 4 experiments).

PAF-induced integrin $\alpha_M\beta_2$ activation (Fig. 3d). Citalopram inhibited sample median fluorescence intensity (M.F.I.) in a concentration-dependent manner (Fig. 3e: $pIC_{50} = 4.02 \pm 0.15$ (N = 6 blood donors)).

The adhesion of PAF-stimulated (1 µM) neutrophils to fibrinogen under static conditions was also investigated to determine if impaired integrin $\alpha_M\beta_2$ activation resulted in a reduction in cell adhesion. As expected, citalopram (0, 10, 20, 50, 100, 200 & 500 µM) inhibited neutrophil adhesion in a concentration-dependent manner (Fig. 3f: $pIC_{50} = 3.88 \pm 0.04$ (N = 10 blood donors)).

The membrane integrity of neutrophils was also assessed to check if impaired functional responses in the presence of citalopram were a result of cell cytotoxicity. Citalopram (0, 10, 20, 50, 100, 200 & 500 µM) had no effect on lactate dehydrogenase (LDH) release (Supplementary Fig. S3: N = 5 blood donors).

Inhibition of neutrophil signalling and function by citalopram closely matched that observed in platelets. Therefore, these data support the hypothesis that citalopram inhibits CalDAG-GEFI-dependent Rap1 nucleotide exchange.

MECHANISM 2: GPVI antagonism. Inhibition of CRPXL-induced Ca^{2+} signalling by citalopram (Fig. 1a,b) is consistent with our previous observations that GPVI-mediated tyrosine phosphorylation of PLCγ2 is inhibited by citalopram[10]. It also suggests that citalopram has a mechanism of action distinct from the inhibition of CalDAG-GEFI-dependent Rap1 nucleotide exchange. Given that citalopram also reduces phosphorylation of FcRγ chain and Src family kinases (SFKs)[10] we hypothesised that citalopram may have a direct effect on GPVI structure and/or function.

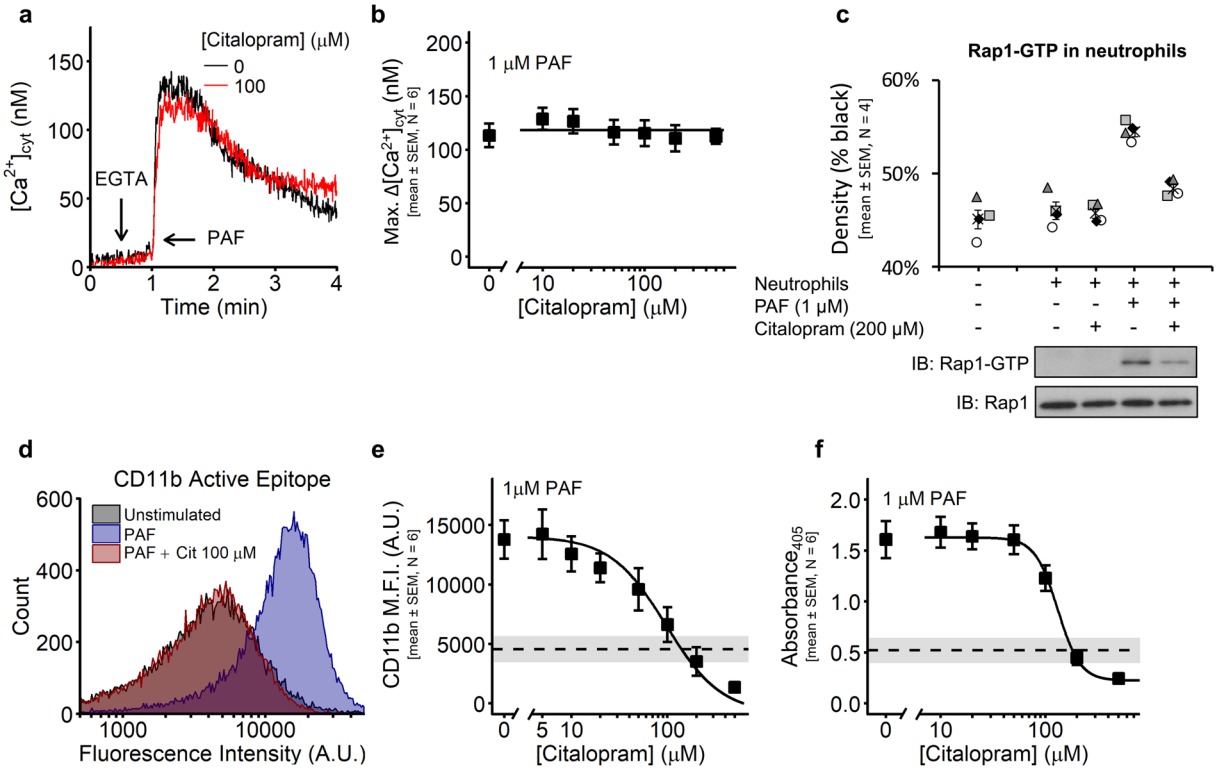

Figure 3. Citalopram inhibits neutrophil functions, despite preserved calcium store release. (**a**,**b**) Calcium (Ca^{2+}) store release was monitored in Fura-2-loaded neutrophils, stimulated with 1 μM platelet-activating factor (PAF). (**a**) Example traces demonstrate PAF-induced increases in the cytosolic concentration of Ca^{2+} ($[Ca^{2+}]_{cyt}$). (**b**) Neutrophils were pre-incubated for approximately 5 min with citalopram (0, 10, 20, 50, 100, 200 & 500 μM) prior to the addition of PAF. The maximum increase in $[Ca^{2+}]_{cyt}$ following PAF addition (Max. $\Delta[Ca^{2+}]_{cyt}$) was recorded (N = 6 blood donors). (**c**) Neutrophils were pre-incubated with (+) or without (−) citalopram (200 μM) for approximately 5 min, followed by either no stimulation (−) or stimulation (+) with 1 μM PAF for 1 min. Rap1-GTP was isolated and quantified using densitometry following SDS-PAGE and Western blotting (N = 4 blood donors. Different donors are indicated by different symbols and the mean by ×). (**d**) Representative histograms, measuring antibody binding to the active epitope of α_M (CD11b) in either unstimulated or PAF-stimulated neutrophils (citalopram = 0 or 100 μM, PAF = 1 μM). (**e**,**f**) A range of citalopram concentrations (0, 5, 10, 20, 50, 100, 200 & 500 μM) were used to create concentration-response curves for the effects of citalopram on (**e**) monoclonal antibody binding to CD11b and (**f**) neutrophil adhesion to fibrinogen (N = 6 blood donors). Dashed line (mean) and grey area (±SEM) indicate (**e**) $\alpha_M\beta_2$ activation or (**f**) fibrinogen-binding in unstimulated neutrophils.

Citalopram inhibits the binding of GPVI antibodies. GPVI is expressed on the surface of platelets in both monomeric and dimeric conformations, although the dimeric form is thought to be particularly important in collagen binding and subsequent platelet activation[13,28]. We hypothesised that citalopram may disrupt the dimeric structure of GPVI, thereby preventing collagen- and CRPXL-induced responses. Experiments were conducted using antibodies that selectively detect either dimeric GPVI (204-11 Fab fragments) or total (dimeric and monomeric) GPVI (HY-101) to determine whether citalopram altered GPVI-dimer expression.

Citalopram reduced the fluorescence intensity (F.I.) of unstimulated platelets labelled with 204-11 Fab fragments and HY-101 antibodies in a concentration-dependent manner (Fig. 4). M.F.I. from platelet samples were fitted to the 4PL model, with the *Max* parameter constrained to the F.I. of the isotype control (Fig. 4b,d: pIC_{50} (204-11) = 4.16 ± 0.03; pIC_{50} (HY-101) = 3.93 ± 0.07 (N = 6 blood donors)). These data suggest that citalopram either reduces total GPVI surface expression or blocks the binding of GPVI antibodies to GPVI. The reduction in HY-101 antibody binding suggests that the effect of citalopram is not specific to dimeric GPVI.

Citalopram-induced inhibition of GPVI-mediated platelet activation is fully reversible. We next investigated whether the impaired GPVI antibody binding caused by citalopram was due to a functionally irreversible mechanism of action such as receptor shedding or internalisation. Platelets were pre-incubated for approximately 5 min with citalopram (0 & 100 μM), which was subsequently removed by pelleting and resuspending platelets in fresh calcium-free Tyrode's (CFT) containing no citalopram (Fig. 5a). Platelets were then stimulated with CRPXL, with or without citalopram, under standard aggregometry conditions.

As expected, citalopram (100 μM) inhibited CRPXL-induced platelet aggregation (Fig. 5c,d). Resuspension of citalopram-treated platelets in fresh CFT restored CRPXL-induced aggregation and the resuspended control and

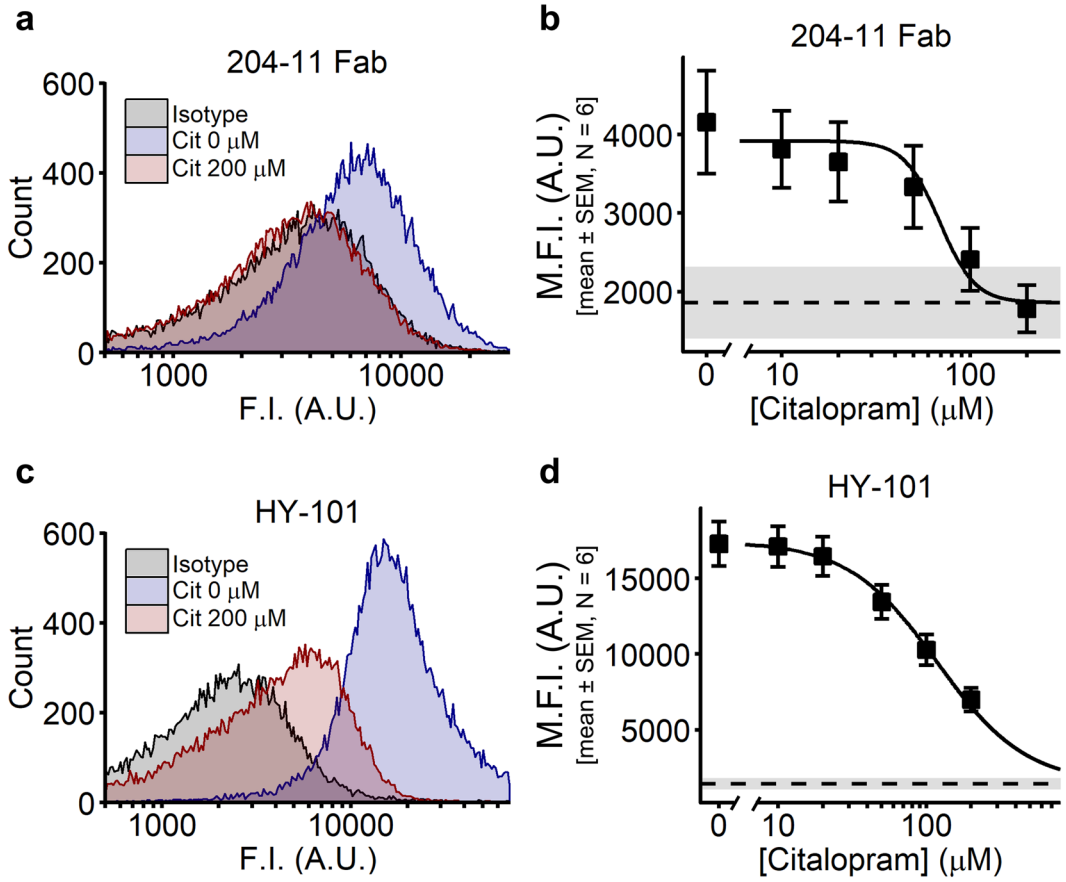

Figure 4. Binding of dimeric anti-glycoprotein VI (GPVI) (204-11 Fab) or total anti-GPVI (HY-101) antibodies to unstimulated platelets. Control Fab or $IgG_{2a}\kappa$ were used as corresponding isotype controls for (**a**,**b**) 204-11 Fab and (**c**,**d**) HY-101, respectively. Example histograms represent the fluorescence intensity (F.I.) of platelets pre-incubated with either a GPVI-specific antibody (blue = 0 μM citalopram, red = 200 μM citalopram), or an isotype control (grey). Sample median F.I. (M.F.I.) was used to generate concentration-response curves, fitted to the four-parameter logistic (4PL) model. Dashed lines (mean) and grey space (±SEM) indicate the M.F.I. of isotype controls, which were used to constrain the *Max* parameter of the 4PL model (N = 6 blood donors).

citalopram-pre-treated platelets responded similarly to CRPXL. Addition of citalopram (100 μM) to pre-treated, pelleted and resuspended platelets inhibited CRPXL-induced aggregation (Fig. 5e,f).

Concentration-response data for the five different conditions were fitted to the 4PL model and CRPXL pEC_{50} values (Fig. 5b) were: (1) untreated = 6.67 ± 0.13; (2) citalopram-treated = 5.35 ± 0.13; (3) untreated and resuspended = 6.58 ± 0.09; (4) citalopram-treated and resuspended = 6.40 ± 0.10; (5) citalopram-treated, resuspended and citalopram-treated = 5.28 ± 0.15; (N = 5 blood donors)). Analysis by 1-way repeated-measures ANOVA (Effect 1 (fixed) = treatment {1,2,3,4,5}; Effect 2 (repeated measure) = donor {N = 5}) indicated a difference between the pEC_{50} values of the five treatments ($P = 1.3 \times 10^{-9}$, F = 63.4, df = 4, 16). A post-hoc Tukey test suggested that there was no difference between the pEC_{50} values of untreated platelets and citalopram-treated platelets following resuspension ($P = 0.59$). Similar results were observed for collagen- and U46619-stimulated platelets (Supplementary Figs S4 and S5).

Citalopram rapidly inhibits CRPXL-induced platelet aggregation in a competitive manner. As shown above, citalopram inhibited the binding of anti-GPVI antibodies and platelet stimulation by CRPXL. However, this latter effect was fully reversible, suggesting that citalopram may bind reversibly to GPVI, thereby preventing binding of the anti-GPVI antibodies and CRP. Such a mechanism would be rapid in onset and competitive in character. We therefore performed additional experiments to investigate the kinetics of onset of platelet inhibition by citalopram, and whether it exhibited a competitive or non-competitive pattern of inhibition.

CRPXL-induced (1 μg mL^{-1}) platelet aggregation was completely inhibited by citalopram (100 μM) following either short pre-incubation times (30, 60 seconds) or on simultaneous addition with CRPXL (i.e., 0 seconds pre-incubation) (Fig. 6a,b). The same result was observed with collagen as an agonist (Supplementary Fig. S6). Following 5 min pre-incubations, citalopram inhibited CRPXL-induced platelet aggregation in a concentration-dependent manner (Fig. 6c,d). Pre-incubating platelets with 20 μM and 50 μM citalopram caused 2.1-fold and 5.3-fold rightward shifts in agonist-response curves, respectively (Fig. 6d). Schild analysis

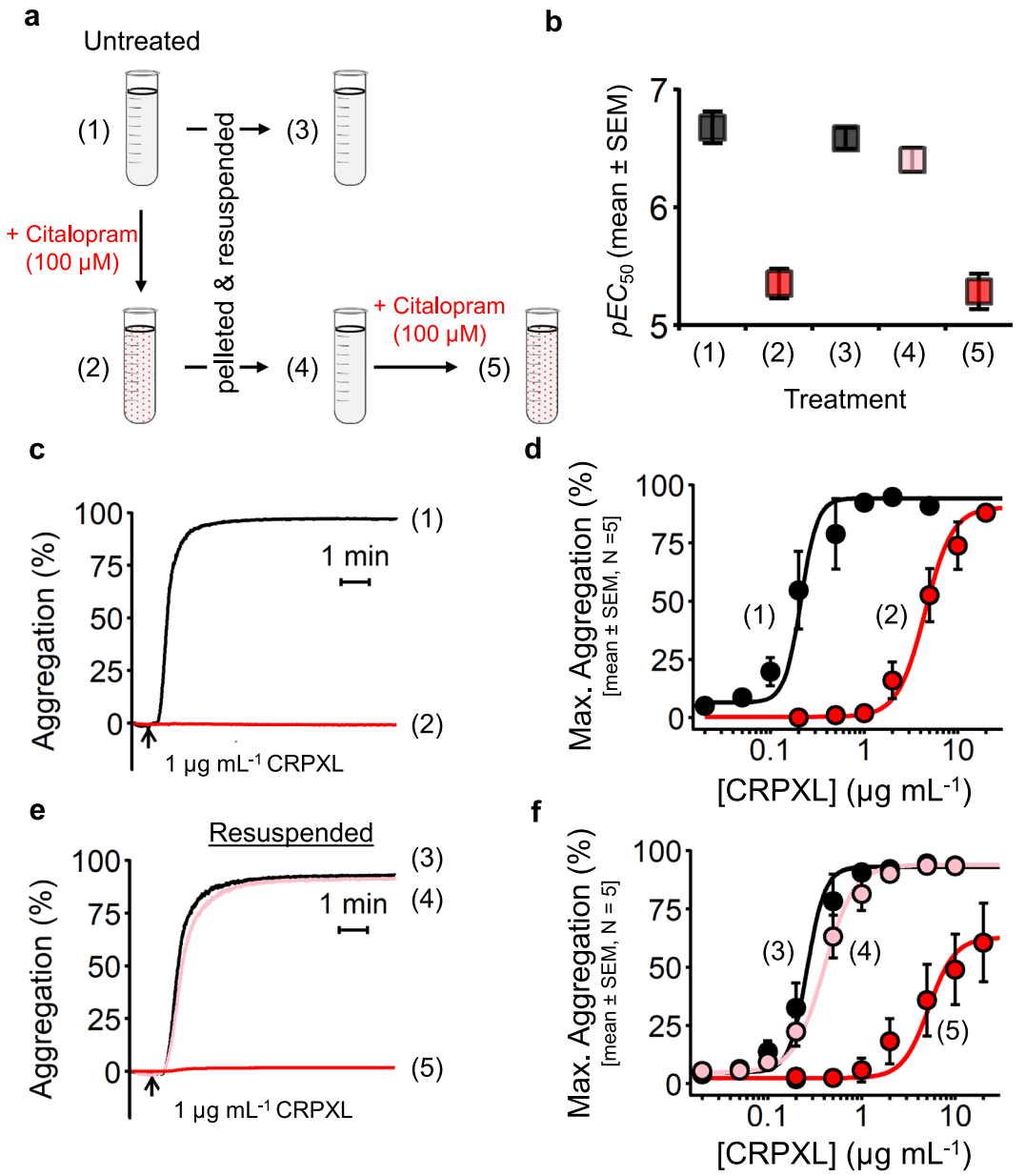

Figure 5. Citalopram inhibition of CRPXL-induced platelet aggregation is reversible. (**a**) Diagram outlining the experimental design to test the reversibility of platelet inhibition by citalopram. Washed platelets were pelleted by centrifugation in the presence of prostaglandin E_1 (PGE_1, 1 µM) and resuspended in fresh calcium-free Tyrode's (CFT). (**b**) pEC_{50} values were derived from the concentration-response curves in (**d**,**f**) (N = 5 blood donors). (**c**,**d**) Two stocks of washed platelets were either untreated (1) or treated with 100 µM citalopram (2). Samples were aliquoted to measure CRPXL-induced aggregation. (**e**,**f**) Stocks (1) and (2) were pelleted and resuspended in fresh CFT and left to rest for 1 hour. Platelet aggregation was then measured in untreated resuspended platelets (3), citalopram-treated resuspended platelets (4), and citalopram-treated resuspended platelets with a second citalopram treatment of 100 µM (5).

(Supplementary Analysis 3) for citalopram concentrations between 5 and 50 µM gave a Schild slope of 1.19 ± 0.09 (N = 6), a result consistent with competitive antagonism. The pA_2 value was 4.79 ± 0.07 indicating a dissociation constant (K_d) of approximately 16 µM. However, 100 µM citalopram caused a 25-fold rightward shift in the agonist-response curve (Fig. 6d). Inclusion of this concentration into the Schild analysis increased the Schild slope to 1.60 ± 0.05 (Fig. 6e). In three experiments, at 200 µM citalopram, there was no response to CRPXL (highest concentration tested = 20 µg mL^{-1}).

These data suggest that at concentrations up to approximately 50 µM, citalopram inhibits CRPXL-induced platelet aggregation in a manner consistent with a competitive mechanism of action. Above this concentration, this pattern breaks down as may be predicted since, at these higher concentrations, citalopram will also exert inhibitory effects via its action on CalDAG-GEFI/Rap1.

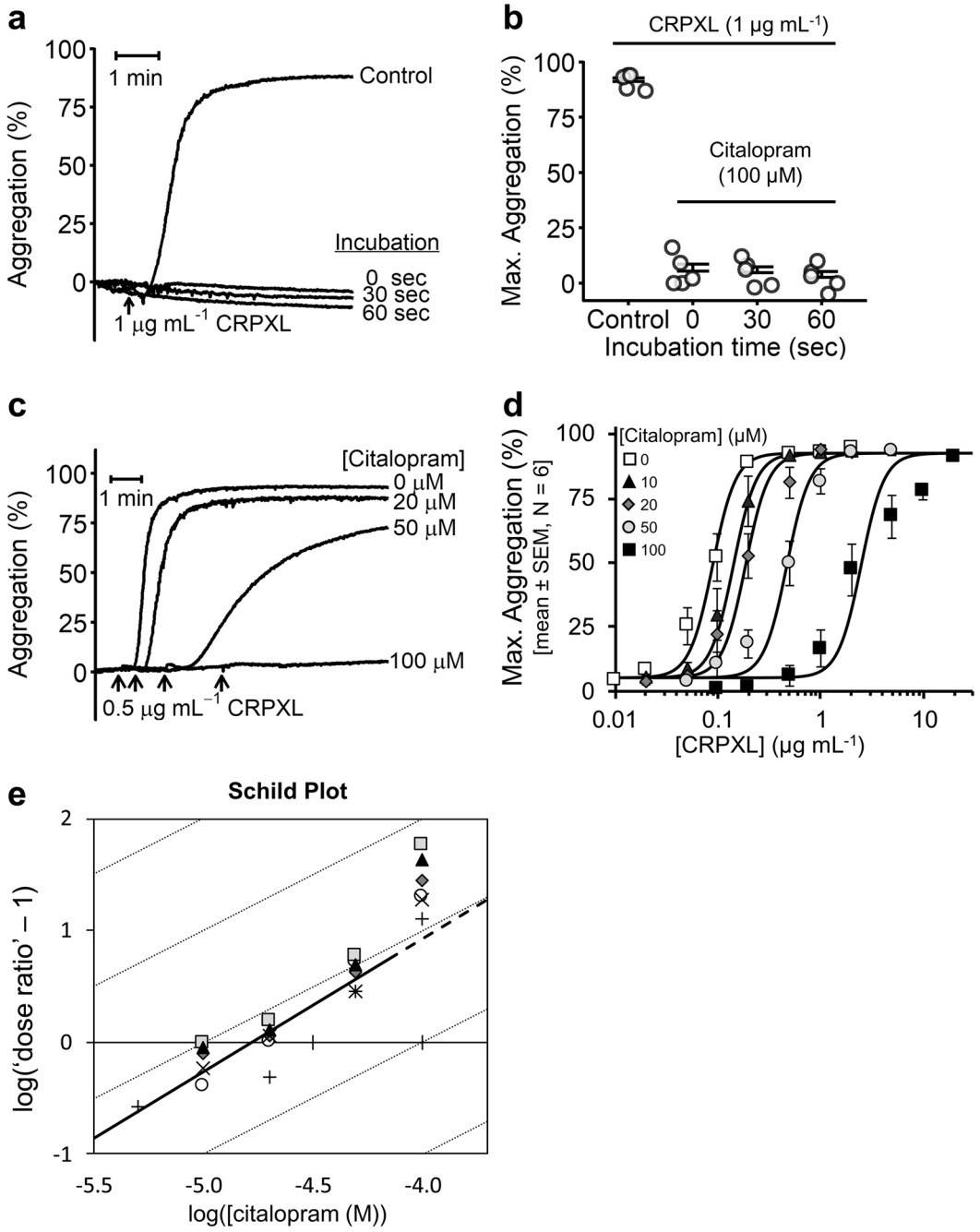

Figure 6. Citalopram instantly and competitively inhibits CRPXL-induced platelet aggregation. (**a**) Representative aggregation traces for either untreated platelets, or platelets pre-incubated with 100 µM citalopram for either 30 or 60 seconds before stimulation with cross-linked collagen-related peptide CRPXL (1 µg mL^{-1}). 0 seconds represents simultaneous addition of citalopram (100 µM) and CRPXL. (**b**) Effect of varying pre-incubation times on the inhibitory effect of citalopram. Following CRPXL (1 µg mL^{-1}) addition, the maximum extent of aggregation over 6 min (Max. Aggregation) was quantified (N = 4 blood donors). (**c**) Example aggregation traces of platelets pre-incubated with citalopram (0, 20, 50, & 100 µM) for approximately 5 min, before stimulation with CRPXL (0.5 µg mL^{-1}). Arrowheads indicate time points of CRPXL addition. (**d**) Agonist concentration-response curves demonstrate how the maximum extent of platelet aggregation (Max. Aggregation) induced by a range of CRPXL concentrations was inhibited by citalopram. Concentrations of citalopram below 10 µM demonstrate similar responses to untreated platelets and were omitted from the figure for clarity. 5 µM citalopram was only tested in a single donor and was therefore omitted from the figure. (**e**) Schild analysis was carried out on a range of citalopram concentrations (5, 10, 20, 50 & 100 µM). Diagonal grey lines have a slope of 1, which corresponds to data expected from a competitive antagonist. The solid line represents the Schild regression line (slope = 1.19 ± 0.09) generated from the data excluding the 100 µM data points. (N = 6 blood donors. Different donors are indicated by different symbols).

Discussion

We have previously shown that citalopram-induced inhibition of platelet function is not caused by blockade of SERT-dependent 5-HT uptake into platelets[10]. The aim of this study was to identify putative SERT-independent mechanisms of platelet inhibition by citalopram. Specifically, we have characterised the effects of citalopram on two distinct processes: (1) Rap1 activation and (2) GPVI receptor function.

In platelets and neutrophils, activation of both TP and PAF receptors respectively induces Ca^{2+} release from intracellular stores via G protein-mediated activation of phospholipase Cβ (PLCβ)[29–31]. In both cell types, citalopram failed to inhibit either U46619- or PAF-induced Ca^{2+} release indicating that the signalling pathways from receptor to elevated $[Ca^{2+}]_{cyt}$ were unaffected by the drug. By contrast, citalopram did block downstream Rap1 activation and cell function. Similarly, Tseng *et al.*[14] reported that ADP-induced platelet aggregation was inhibited by citalopram, but not ADP-induced Ca^{2+} signalling. Notably, Ca^{2+}-dependent Rap1 activation in both platelets and neutrophils is mediated by CalDAG-GEFI[15,21]. Our results from an *in vitro* fluorescence-based binding assay show citalopram inhibits CalDAG-GEFI-mediated nucleotide exchange of Rap1B. The recovery of CRPXL-, collagen- and U46619-induced aggregation after washing out citalopram (Fig. 5, Supplementary Figs S4 and S5) indicates that this inhibition by citalopram is reversible. We therefore propose that citalopram binds directly and reversibly to either CalDAG-GEFI, Rap1 or a complex of both, thereby inhibiting Rap1 activation.

Comparatively few studies have reported the *in vitro* effects of SSRIs on neutrophils. Although fluoxetine has previously been shown to inhibit some neutrophil functions[22], we believe that ours is the first report of citalopram inhibiting human neutrophil function. Unlike platelets, neutrophils do not express SERT[32]. Therefore, our results provide further confirmation of a direct and SERT-independent mechanism of action of citalopram in neutrophils and, by extension, platelets.

We have previously reported that citalopram inhibited collagen-induced aggregation and phosphorylation of molecules in the GPVI signalling pathway[10]. We now report that citalopram also inhibits platelet aggregation induced by CRPXL, a GPVI-selective agonist, and reduces the binding of anti-GPVI antibodies to unstimulated platelets. One possible explanation for these results is a reduction in surface receptor number, either by shedding or internalisation. However, for a full agonist, a reduction in receptor number is predicted to reduce the observed potency of the agonist[33], and this has previously been demonstrated for CRPXL-induced aggregation in platelets with 50% levels of GPVI[34]. Thus, the similarity in CRPXL responsiveness of untreated resuspended platelets (Fig. 5f, condition (3)) and citalopram-pre-treated resuspended platelets (Fig. 5f, condition (4)) suggests that little if any GPVI was lost from the platelet surface as a result of citalopram treatment. Moreover, our data show that inhibition of CRPXL-induced platelet aggregation by citalopram is both instantaneous in onset and fully reversible. Taken together, these data strongly support a reversible, competitive mechanism of action for citalopram, rather than a reduction in surface receptor expression. We therefore propose that citalopram binds directly to GPVI-FcRγ chain complex, thereby preventing collagen- and CRPXL-induced platelet activation.

Our proposal that citalopram exerts two distinct mechanisms of action is further supported by the observed inhibitory potencies of citalopram in our studies. The Schild analysis indicates that citalopram binds to GPVI/FcRγ chain with a K_d of approximately 16 μM. This is wholly consistent with data reported in our previous study[10] showing that 20 μM citalopram caused an approximate 2-fold rightward shift of the collagen concentration-response curve but had no discernible effect on U46619-induced aggregation. pIC_{50} values for inhibition of GPVI-independent functions: aggregation induced by U46619 (4.15 ± 0.27) and ionomycin (3.98 ± 0.09); PAF-induced activation of neutrophil $\alpha_M\beta_2$ (4.02 ± 0.15); adhesion of platelets (4.00 ± 0.07) and neutrophils (3.88 ± 0.04) to fibrinogen; and CalDAG-GEFI-dependent Rap1B activation (3.67 ± 0.32), are all consistent with citalopram binding to and inhibiting CalDAG-GEFI/Rap1B at a concentration of approximately 100 μM. This is further reflected by the Schild analysis showing a rightward shift in the CRPXL concentration-response curves consistent with competitive antagonism at citalopram concentrations up to 50 μM, whereas at higher concentrations the shift was greater (Fig. 6) caused by the combination of the two distinct inhibitory mechanisms outlined above.

Citalopram may inhibit platelets and neutrophils through other unidentified mechanisms that are distinct from SERT blockade. For example, Bonnin *et al.*, (2012)[35] have proposed that (*R*)-citalopram, the lower potency isomer[36], may act via the orphan sigma-1 receptor. However, as we have previously noted, this is unlikely to be the mechanism responsible for the action of citalopram in platelets[10].

In summary, we propose a model (Fig. 7) in which citalopram binds to two distinct molecular targets: (1) GPVI/FcRγ chain ($K_d \approx 16$ μM) and (2) CalDAG-GEFI/Rap1B ($K_d \approx 100$ μM). This model predicts that citalopram would selectively disrupt GPVI-dependent platelet activation at concentrations between 20 and 50 μM, and above 50 μM, it would also inhibit Ca^{2+}-dependent functions mediated through CalDAG-GEFI. These two novel, putative and distinct inhibitory mechanisms of action: (1) competitive antagonism of GPVI-FcRγ chain inhibition and (2), inhibition of CalDAG-GEFI-mediated nucleotide exchange of Rap1B, both need much higher concentrations of citalopram than are required to inhibit SERT, its primary mechanism of action. Hence, these effects are unlikely to be of clinical significance[10], either as a cause of reported bleeding complications[37–41], or as a strategy for reducing cardiovascular disease. Further studies will be required to confirm these putative mechanisms. However, if confirmed, citalopram may prove to be a useful investigative tool for the study of CalDAG-GEFI, Rap1, and GPVI signalling, as well as a practical chemical starting point for the discovery of more selective and potent inhibitors. A potent, selective GPVI antagonist could be a potentially useful anti-thrombotic agent and inhibitors of CalDAG-GEFI/Rap1 may have a wide range of uses in haematopoietic cells.

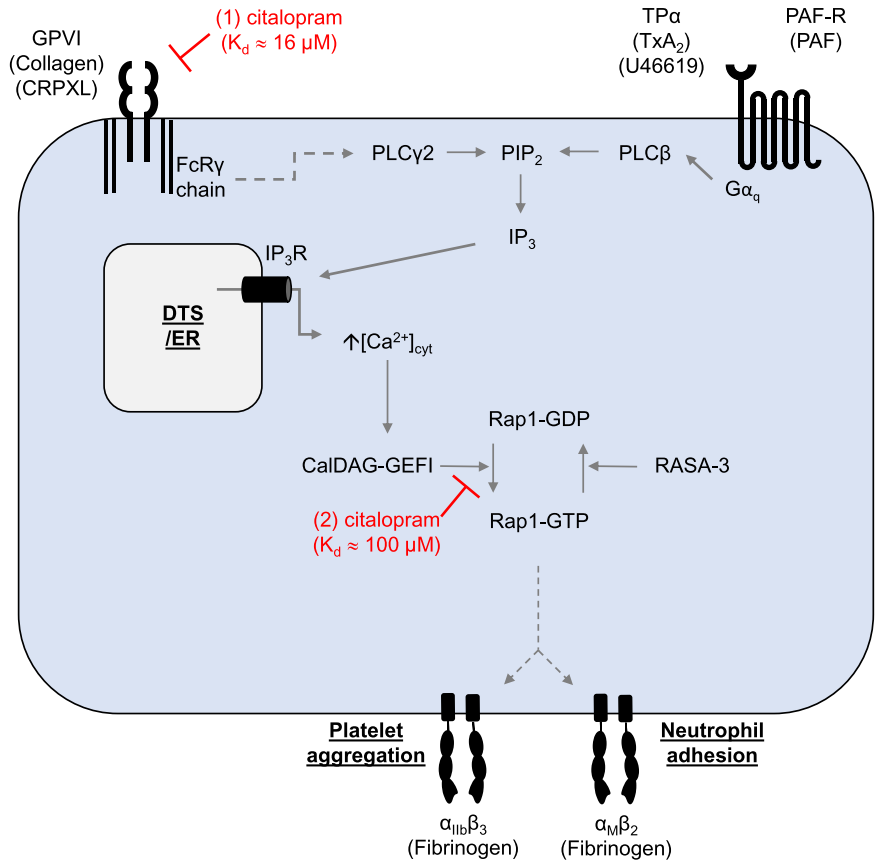

Figure 7. Two novel, putative mechanisms of action for citalopram-induced platelet and neutrophil inhibition. (1) In platelets, citalopram binds to the GPVI/FcRγ chain complex (K_d ≈ 16 μM), thereby acting as a competitive antagonist and blocking receptor activation by the GPVI agonists CRPXL and collagen. This prevents activation of phospholipase Cγ2 (PLCγ2), generation of inositol trisphosphate (IP_3), activation of IP_3 receptors (IP_3R) and subsequent release of calcium from the dense tubular system (DTS) or endoplasmic reticulum (ER) into the cytoplasm. (2) In both platelets and neutrophils, at higher concentrations, citalopram interacts with CalDAG-GEFI/Rap1B (K_d ≈ 100 μM), thereby inhibiting the Ca^{2+}- and CalDAG-GEFI-dependent conversion of Rap1B-GDP to Rap1B-GTP. (In platelets, Ras GTPase-activating protein 3 (RASA-3) mediates the conversion of Rap1B-GTP to Rap1B-GDP[51]). This model explains how citalopram can selectively disrupt GPVI-dependent platelet activation at concentrations between 20 and 50 μM, while inhibiting the CalDAG-GEFI/Rap1 signalling axis at concentrations above 50 μM in both platelets and neutrophils.

Material and Methods

Materials. Prostaglandin E_1 (PGE_1), indomethacin, U46619, citric acid, trisodium citrate, ionomycin, glycerol, dextran-500, Nonidet P-40 (NP-40), fibrinogen, p-nitrophenyl phosphate (pNPP) and Percoll® were from Sigma (Poole, U.K.). Ethylene glycol-bis(2-aminoethyl ether)-*N*,*N*,*N*',*N*'-tetraacetic acid (EGTA) was from Calbiochem (Nottingham, U.K.). BODIPY-FL-GDP, dithiothreitol, fluorescein (FITC)-conjugated anti-CD15 and allophycocyanin (APC)-conjugated anti-CD11b/CD18 antibodies were from Thermo Fisher Scientific, (Loughborough, U.K.). Alexa488-conjugated anti-mouse $F(ab)_2$ was from Jackson ImmunoResearch (Ely, U.K.). Murine $IgG_{2aκ}$ isotype control antibody was from BioLegend (London, U.K.). (*RS*)-citalopram and PAF were from Cambridge Bioscience (Cambridge, U.K.). Horm® collagen was from Takeda (Linz, Austria). Bovine serum albumin (BSA) was from GE Healthcare (Buckinghamshire, U.K.). Fura-2 (AM) was from TEFLabs (Cambridge, U.K.). CRPXL was synthesised in the laboratory of Professor Richard Farndale (University of Cambridge, U.K.).

Blood donation. Donation of fresh blood from healthy, consenting human volunteers was approved by the University of Cambridge Human Biology Research Ethics Committee (Ref: HBREC.2015.18). Prior to any blood donation, informed consent was obtained from each blood donor. The consent form was signed by both the donor and one of the project supervisors (G.E.J. or S.O.S.). A fresh consent form is signed annually. On the occasion of each donation of blood, a donation record form was signed by both the donor and the phlebotomist (G.E.J., S.O.S. or H.G.R.). Collection of blood from donors, its use and subsequent disposal were performed in accordance with relevant guidelines and regulations. Blood was drawn into 50 mL syringes containing trisodium citrate (final concentration of 11 mM in blood).

Washed platelet preparation. Citrated blood was centrifuged (500 × g, 5 min) to obtain platelet-rich plasma (PRP). Following addition of PGE_1 (final concentration of 1 μM), PRP was centrifuged (900 × g, 15 min)

and the resulting platelet pellet resuspended in a modified calcium-free Tyrode's buffer (CFT; 137 mM NaCl, 11.9 mM $NaHCO_3$, 0.4 mM NaH_2PO_4, 2.7 mM KCl, 1.1 mM $MgCl_2$, 5.6 mM glucose; pH = 7.4). Platelet counts were adjusted to $2 \times 10^8\,mL^{-1}$ using a Z2 Coulter particle counter (Beckman Coulter, High Wycombe, U.K.).

Neutrophil preparation. Citrated blood was mixed 2:1 with a saline solution of dextran-500 (final concentration of 1% [w/v]) and left for 30 min to allow red blood cell (RBC) sedimentation, whilst retaining white blood cells (WBCs) within the PRP. WBC-rich PRP was aspirated and layered over a discontinuous density gradient of Percoll® (1.5 mL of 1.088 g mL^{-1} Percoll®, carefully layered on top of 1.5 mL of 1.100 g mL^{-1} Percoll®). Samples were centrifuged (600 × g, 20 min) to separate granulocytes from the lower-density platelets, lymphocytes and monocytes. The isolated granulocyte band was aspirated, washed with phosphate-buffered saline (PBS), centrifuged (300 × g, 5 min) and resuspended in CFT. The cell concentration was adjusted to $1 \times 10^6\,mL^{-1}$ using a Z2 Coulter particle counter (Beckman Coulter, High Wycombe, U.K.).

Platelet aggregometry. Platelet aggregation was measured by turbidimetric aggregometry as previously described[10,42] using two Aggregation Remote Analyzer Modules (AggRAM) with HemoRAM software (v1.2) (Helena Biosciences, Newcastle, U.K.). Washed platelets (WP) (247.5 µL, $2 \times 10^8\,mL^{-1}$) were aliquoted into glass cuvettes containing magnetic stir bars. 2.5 µL agonist was added and aggregation recorded at 37 °C with a stir speed of 1,000 rpm. The maximum extent of aggregation over 6 min was determined as previously described[43].

Monitoring cytosolic calcium concentration. Changes in the cytosolic concentration of Ca^{2+} ($[Ca^{2+}]_{cyt}$) were monitored using the fluorescent Ca^{2+} indicator, Fura-2. PRP or isolated neutrophils were incubated for 30 min at 37 °C with 2.5 µM Fura-2 AM. With PRP, WP preparation was subsequently continued as described above. Fura-2-loaded neutrophils were centrifuged (300 × g, 5 min) and resuspended in fresh CFT to $1 \times 10^6\,mL^{-1}$. Fura-2 fluorescence was measured using a Cairn Optoscan Spectrophotometer and Acquisition Engine (v1.1.7) (Cairn Research, Faversham, U.K.) in stirred 1.2 mL samples of WP or neutrophils at 37 °C. Following chelation of extracellular Ca^{2+} by EGTA (10 mM), agonist-induced changes in $[Ca^{2+}]_{cyt}$ were monitored for 3 min. $[Ca^{2+}]_{cyt}$ was calculated using the method of Grynkiewicz *et al.*[44]. The agonist-induced response (peak $[Ca^{2+}]$) was obtained by subtracting the basal $[Ca^{2+}]_{cyt}$ from the peak signal.

Rap1 activation and Western Blot. Rap1 activation was measured using an Active Rap1 Pull-Down and Detection Kit (Thermo Fisher Scientific, Loughborough, U.K.). 247.5 µL of either WP ($2 \times 10^8\,mL^{-1}$) or neutrophils ($1 \times 10^6\,mL^{-1}$) were stimulated in AggRAM aggregometers for 1 min with either CRPXL (0.5 µg mL^{-1}), U46619 (0.2 µM) or PAF (1 µM). Reactions were terminated with 1:1 lysis/binding/wash buffer (LBW: 25 mM Tris HCl, 150 mM NaCl, 5 mM $MgCl_2$, 1% [v/v] NP-40, 5% [v/v] glycerol, pH = 7.2). Lysates were put on ice for 5 min, followed by centrifugation (8,000 × g, 1 min) to remove cellular debris. For total Rap1 quantification, 20 µL of each sample lysate was aliquoted into 1:1 Laemmli buffer (final concentrations: 62.5 mM Tris HCl, 1% [v/v] glycerol, 2% [w/v] SDS, 2.5% [v/v] mercaptoethanol, 0.025% [w/v] brilliant blue). For active Rap1 (i.e., Rap1-GTP) quantification, the remaining 480 µL sample was aliquoted into filter spin cups containing 100 µL of 50% glutathione-agarose beads and 20 µg of GST-RalGDS-RBD fusion protein. Samples were briefly vortexed then incubated with gentle rocking (1 hour, 4 °C). Samples were centrifuged (8,000 × g, 1 min) and washed 3 times with 400 µL LBW, before the addition of 50 µL Laemmli buffer. Samples were then centrifuged (8,000 × g, 2 min) through the spin cups to obtain bead-free samples for Western blot analysis.

Total Rap1 and Rap1-GTP samples underwent SDS PAGE and Western blot analysis. Samples were added to 10 well 4–12% pre-cast NuPage Bis-Tris gels (Invitrogen, Paisley, U.K.), followed by SDS/PAGE separation and transfer to PVDF membranes (Millipore, Watford, U.K.). Membranes were incubated with Rap1 primary antibodies (Thermo Fisher Scientific, Loughborough, U.K) followed by incubation with HRP-conjugated secondary antibodies (Dako, Ely, U.K.). Enhanced chemiluminescence (ECL) and X-ray hyperfilm® (Amersham Biosciences, Buckinghamshire, U.K.) were used to detect protein bands. Developed X-ray films were scanned, and unprocessed images analysed using ImageJ (v1.50) as follows: identical areas (height (100) × width (150) = 15,000 pixels) were drawn around each protein band and the density of all pixels (scale 0–255 each) summed. The density of each area was therefore quantified on a scale from 0 (totally white) to 3,825,000 (totally black). Values are presented as % black. Uncropped images of X-ray films used for quantification of Rap1-GTP are shown in Supplementary Figs S7 and S8.

Monitoring Rap1 nucleotide exchange activity. The rate of Rap1 nucleotide exchange was measured using a fluorescence-based *in vitro* enzyme assay[17,45,46]. 100 µL of reaction buffer (20 mM Tris base, 150 mM NaCl, 5 mM $MgCl_2$, 2 mM dithiothreitol, 10% [v/v] glycerol, 0.08% [v/v] NP-40, 1 µM Rap1B, 0.1 µM BODIPY-FL-GDP, pH = 7.5) was aliquoted into wells of a Nunc F96 well, black, flat-bottomed plate and the baseline fluorescence intensity (F.I.) recorded (excitation 485 nm; emission 520 nm) for 3 min with a Fluostar Optima plate reader (BMG Labtech, Aylesbury, U.K.). Measurements were halted and CalDAG-GEFI (0.3 µM) added to increase the rate of BODIPY-FL-GDP exchange onto Rap1, thereby increasing F.I. Recording was resumed and the average F.I. prior to CalDAG-GEFI addition subtracted from the final F.I. 20 min after the addition of CalDAG-GEFI (ΔF.I.).

Rap1B and CalDAG-GEFI were cloned from human genes into a protein expression vector p15LIC2 6xHis, which was purified in *E. coli*, as previously described[17]. Both proteins contained a C-terminal truncation (p.(Lys168_Leu184del) and p.(Ala552_Leu609del), respectively) which removed disordered regions to improve stability during the purification process, while leaving all the functional domains intact. Protein sequences (native and recombinant mutants) for both Rap1B and CalDAG-GEFI are shown in Supplementary Fig. S9.

Neutrophil integrin $\alpha_M\beta_2$ activation. Neutrophil integrin $\alpha_M\beta_2$ (Mac-1, CD11b/CD18) activation was measured using an APC-conjugated monoclonal antibody, which binds the activated epitope of integrin α_M

(CD11b). Neutrophils (100 µL, 1×10^6 mL^{-1}) were incubated with the active CD11b antibody in the absence of light (5 min, 4 °C). Samples were fixed with 2% [v/v] paraformaldehyde and neutrophils gated by forward scatter (FSC), side scatter (SSC) and CD15$^+$ criteria. The median fluorescence intensity (M.F.I.) of activated CD11b from 30,000 gated events was then determined for each sample using an Accuri™ C6 flow cytometer (BD Bioscience, Oxford, U.K.).

Neutrophil adhesion. The adhesion of neutrophils to fibrinogen under static conditions was quantified by adapting a protocol developed to measure levels of cell-derived acid phosphatase (EC 3.1.3.2)[47]. Immulon-2HB 96 flat-bottom well plates (Thermo Fisher Scientific, Loughborough, U.K.) were incubated overnight at 4 °C with 100 µL of fibrinogen (10 µg mL^{-1} in saline). Excess ligand was discarded, and wells blocked with 175 µL BSA (5% [w/v] in CFT) for 1 hour. Wells were washed three times with BSA (0.1% [w/v] in CFT). 50 µL of isolated neutrophils (4.00×10^6 mL^{-1}) were added to wells and left for 1 hour at room temperature. Samples were discarded, and the wells washed as before, followed by the addition of 150 µL of citrate lysis buffer (3.53 mM pNPP, 71.4 mM trisodium citrate, 28.55 mM citric acid, 0.1% [v/v] Triton X-100; pH 5.4). After 1 hour, 100 µL of 2 M NaOH was added and absorbance measured at 405 nm with a Sunrise™ plate reader (Tecan, Reading, U.K.).

Lactate dehydrogenase cytotoxicity assay. LDH release from neutrophils was measured to determine drug-induced cytotoxicity and cytolysis, using a Pierce LDH Activity Assay Kit (Thermo Fisher Scientific, Loughborough, U.K.). Neutrophils (250 µL, 1×10^6 mL^{-1}) were centrifuged (8,000 × g, 1 min) and 50 µL of supernatant was aliquoted into wells of an Immulon-2HB 96-well flat-bottom plate. 50 µL of the proprietary reaction mixture (Thermo Fisher, product code: 1862887) was added to each well for 30 min. 50 µL of the proprietary stop solution (Thermo Fisher, product code: 1862880) terminated the reaction and background absorbance at 680 nm was subtracted from the absorbance at 490 nm. Measurements were made using a Sunrise™ plate reader (Tecan, Reading, U.K.).

Antibody Binding to Glycoprotein VI. The binding of antibodies to dimeric or total (dimeric and monomeric) platelet GPVI was quantified as previously described using 204-11 Fab[48] and HY-101[49] antibodies, respectively. WP (2.50×10^7 mL^{-1}) were incubated for 10 min with either HY-101 (5 µg mL^{-1}) or 204-11 Fab (10 µg mL^{-1}). Murine IgG$_{2a}$κ or Fab were used as corresponding isotype controls, respectively. 5 µg mL^{-1} of Alexa488-conjugated anti-mouse F(ab)$_2$ was subsequently added and incubated in the dark for 10 min. Samples were diluted 1:8 in CFT and the M.F.I. measured using an Accuri™ C6 flow cytometer (BD Bioscience, Oxford, U.K.).

Data and statistical analysis. Concentration-response data were modelled using a four-parameter logistic (4PL) model[43,50]:

$$R_{PRED} = \frac{Min - Max}{1 + ([A]/10^{-pA_{50}})^{n_H}} + Max$$

Where: R_{PRED} = predicted response (dependent variable); $[A]$ = agent concentration (independent variable); Min = response when $[A] = 0$; Max = response when $[A] = \infty$; pA_{50} = -log $[A]$ (expressed in units of mol L^{-1}, or g mL^{-1} for CRPXL) when $R_{PRED} = (Max + Min)/2$; n_H = Hill coefficient. When A is an inhibitor, the pA_{50} is the pIC_{50}. Unless otherwise stated, fitting was performed using minimisation of least squares with the Solver function in Microsoft® Excel. Data are presented as mean ± standard error of the mean (SEM). Figures were generated using either R 3.3.2 (The R Foundation for Statistical Computing, Vienna, Austria) or Microsoft® Excel. Additional statistical analyses are presented in Supplementary Methods.

References

1. Bullard, I. *Prescriptions Dispensed in the Community, England 2006 to 2016.* (NHS Digital, 2017).
2. Blakely, R. D. *et al.* Cloning and expression of a functional serotonin transporter from rat brain. *Nature* **354**, 66–70 (1991).
3. Hoffman, B. J., Mezey, E. & Brownstein, M. J. Cloning of a serotonin transporter affected by antidepressants. *Science* **254**, 579–580 (1991).
4. Hyttel, J. Citalopram pharmacological profile of a specific serotonin uptake inhibitor with antidepressant activity. *Prog. Neuropsychopharmacol. Biol. Psychiatry* **6**, 277–295 (1982).
5. Owens, M. J. Selectivity of antidepressants: From the monoamine hypothesis of depression to the SSRI revolution and beyond. *J. Clin. Psychiatry* **65**, 5–10 (2004).
6. Goubau, C., Buyse, G. M., Di Michele, M., Van Geet, C. & Freson, K. Regulated granule trafficking in platelets and neurons: A common molecular machinery. *Eur. J. Paediatr. Neurol.* **17**, 117–125 (2013).
7. Maurer-Spurej, E., Pittendreigh, C. & Solomons, K. The influence of selective serotonin reuptake inhibitors on serotonin metabolism in human platelets. *Thromb. Haemost.* **91**, 119–128 (2004).
8. Lopez-Vilchez, I. *et al.* Escitalopram impairs thrombin-induced platelet response, cytoskeletal assembly and activation of associated signalling pathways. *Thromb. Haemost.* **117**, 2312–2321 (2017).
9. Tseng, Y. L. *et al.* A selective serotonin reuptake inhibitor, citalopram, inhibits collagen-induced platelet aggregation and activation. *Thromb. Res.* **126**, 517–523 (2010).
10. Roweth, H. G. *et al.* Citalopram inhibits platelet function independently of SERT-mediated 5-HT transport. *Sci. Rep.* **8**, 3494 (2018).
11. Carneiro, A. M. D., Cook, E. H., Murphy, D. L. & Blakely, R. D. Interactions between integrin αIIbβ3 and the serotonin transporter regulate serotonin transport and platelet aggregation in mice and humans. *J. Clin. Invest.* **118**, 1544–1552 (2008).
12. Galan, A. M. *et al.* Serotonergic mechanisms enhance platelet-mediated thrombogenicity. *Thromb. Haemost.* **102**, 511–519 (2009).
13. Jung, S. M. *et al.* Constitutive dimerization of glycoprotein VI (GPVI) in resting platelets is essential for binding to collagen and activation in flowing blood. *J. Biol. Chem.* **287**, 30000–30013 (2012).
14. Tseng, Y. L., Chiang, M. L., Lane, H. Y., Su, K. P. & Lai, Y. C. Selective serotonin reuptake inhibitors reduce P2Y$_{12}$ receptor-mediated amplification of platelet aggregation. *Thromb. Res.* **131**, 325–332 (2013).
15. Crittenden, J. R. *et al.* CalDAG-GEFI integrates signaling for platelet aggregation and thrombus formation. *Nat. Med.* **10**, 982–986 (2004).

16. Stefanini, L. & Bergmeier, W. RAP1-GTPase signaling and platelet function. *J. Mol. Med.* **94**, 13–19 (2016).
17. Cook, A. A. *et al.* Calcium-induced structural rearrangements release autoinhibition in the Rap-GEF, CalDAG-GEFI. *J. Cell Biol.* **293**, 8521–8529 (2018).
18. Lee, H. S., Lim, C. J., Puzon-McLaughlin, W., Shattil, S. J. & Ginsberg, M. H. RIAM activates integrins by linking talin to Ras GTPase membrane-targeting sequences. *J. Biol. Chem.* **284**, 5119–5122 (2009).
19. Moser, M., Legate, K. R., Zent, R. & Fassler, R. The tail of integrins, talin, and kindlins. *Science* **324**, 895–899 (2009).
20. M'Rabet, L. *et al.* Activation of the small GTPase Rap1 in human neutrophils. *Blood* **92**, 2133–2140 (1998).
21. Bergmeier, W. *et al.* Mice lacking the signaling molecule CalDAG-GEFI represent a model for leukocyte adhesion deficiency type III. *J. Clin. Invest.* **117**, 1699–1707 (2007).
22. Strümper, D. *et al.* Effects of antidepressants on function and viability of human neutrophils. *Anesthesiology* **98**, 1356–1362 (2003).
23. Burkhart, J. M. *et al.* The first comprehensive and quantitative analysis of human platelet protein composition allows the comparative analysis of structural and functional pathways. *Blood* **120**, e73–e82 (2012).
24. Filippi, M. D. Leukocyte transcellular diapedesis: Rap1b is in control. *Tissue Barriers* **3**, 1–8 (2015).
25. Kumar, S. *et al.* The small GTPase Rap1b negatively regulates neutrophil chemotaxis and transcellular diapedesis by inhibiting Akt activation. *J. Exp. Med.* **211**, 1741–1758 (2014).
26. Caron, E., Self, A. J. & Hall, A. The GTPase Rap1 controls functional activation of macrophage integrin αMβ2 by LPS and other inflammatory mediators. *Curr. Biol.* **10**, 974–978 (2000).
27. Yakubenko, V. P. *et al.* Identification of the Binding Site for Fibrinogen Recognition Peptide γ383-395 within the α_MI-Domain of Integrin $\alpha_M\beta_2$. *J. Biol. Chem.* **276**, 13995–14003 (2001).
28. Poulter, N. S., Pollitt, A. Y., Owen, D. M., Gardiner, E. E. & Andrews, R. K. Clustering of glycoprotein VI (GPVI) dimers upon adhesion to collagen as a mechanism to regulate GPVI signaling in platelets. *J. Thromb. Haemost.* **15**, 549–564 (2017).
29. Kinsella, B. T., O'Mahony, D. J. & Fitzgerald, G. A. The human thromboxane A_2 receptor α isoform (TP_α) functionally couples to the G proteins G_q and G_{11} *in vivo* and is activated by the isoprostane 8-epi prostaglandin $F_{2\alpha}$. *J. Pharmacol. Exp. Ther.* **281**, 957–64 (1997).
30. Paul, B. Z. S., Jin, J. & Kunapuli, S. P. Molecular Mechanism of Thromboxane A_2-induced Platelet Aggregation. *J. Biol. Chem.* **274**, 29108–29114 (1999).
31. Honda, Z., Ishii, S. & Shimizu, T. Platelet-activating factor receptor. *J. Biochem.* **131**, 773–779 (2002).
32. Herr, N., Bode, C. & Duerschmied, D. The effects of serotonin in immune cells. *Front. Cardiovasc. Med.* **4**, 1–11 (2017).
33. Black, J. W., Leff, P., Shankley, N. P. & Wood, J. An operational model of pharmacological agonism: the effect of E/[A] curve shape on agonist dissociation constant estimation. *Br. J. Pharmacol.* **84**, 561–571 (1985).
34. Snell, D. C. *et al.* Differential effects of reduced glycoprotein VI levels on activation of murine platelets by glycoprotein VI ligands. *Biochem. J.* **368**, 293–300 (2002).
35. Bonnin, A., Zhang, L., Blakely, R. D. & Levitt, P. The SSRI citalopram affects fetal thalamic axon responsiveness to netrin-1 *in vitro* independently of SERT antagonism. *Neuropsychopharmacology* **37**, 1879–1884 (2012).
36. Owens, M. J., Knight, D. L. & Nemeroff, C. B. Second-generation SSRIs: human monoamine transporter binding profile of escitalopram and *R*-fluoxetine. *Biol. Psychiatry* **50**, 345–350 (2001).
37. van Walraven, C., Mamdani, M. M., Wells, P. S. & Williams, J. I. Inhibition of serotonin reuptake by antidepressants and retrospective cohort study. *Br. Med. J.* **323**, 1–6 (2001).
38. Dalton, S. O. *et al.* Use of selective serotonin reuptake inhibitors and risk of upper gastrointestinal tract bleeding. *Arch. Intern. Med.* **163**, 59–64 (2003).
39. Opatrny, L., Delaney, J. A. C. & Suissa, S. Gastro-intestinal haemorrhage risks of selective serotonin receptor antagonist therapy: A new look. *Br. J. Clin. Pharmacol.* **66**, 76–81 (2008).
40. Dall, M. *et al.* An association between selective serotonin reuptake inhibitor use and serious upper gastrointestinal bleeding. *Clin. Gastroenterol. Hepatol.* **7**, 1314–1321 (2009).
41. Hackam, D. G. & Mrkobrada, M. Selective serotonin reuptake inhibitors and brain hemorrhage. *Neurology* **79**, 1862–1865 (2012).
42. Jarvis, G. E. Platelet aggregation: turbidimetric measurements. *Methods Mol. Biol.* **272**, 65–76 (2004).
43. Jarvis, G. E., Humphries, R. G., Robertson, M. J. & Leff, P. ADP can induce aggregation of human platelets *via* both $P2Y_1$ and P_{2T} receptors. *Br. J. Pharmacol.* **129**, 275–282 (2000).
44. Grynkiewicz, G., Poenie, M. & Tsien, R. Y. A new generation of Ca^{2+} indicators with greatly improved fluorescence properties. *J. Biol. Chem.* **260**, 3440–3450 (1985).
45. Lozano, M. L. *et al.* Novel mutations in RASGRP2, which encodes CalDAG-GEFI, abrogate Rap1 activation, causing platelet dysfunction. *Blood* **128**, 1282–1289 (2016).
46. Ren, J., Cook, A. A., Bergmeier, W. & Sondek, J. A negative-feedback loop regulating ERK1/2 activation and mediated by RasGPR2 phosphorylation. *Biochem. Biophys. Res. Commun.* **474**, 193–198 (2016).
47. Bellavite, P. *et al.* A colorimetric method for the measurement of platelet adhesion in microtiter plates. *Anal. Chem.* **216**, 444–450 (1994).
48. Jung, S. M., Tsuji, K. & Moroi, M. Glycoprotein (GP) VI dimer as a major collagen-binding site of native platelets: direct evidence obtained with dimeric GPVI-specific Fabs. *J. Thromb. Haemost.* **7**, 1347–1355 (2009).
49. Chen, H., Locke, D., Liu, Y., Liu, C. & Kahn, M. L. The platelet receptor GPVI mediates both adhesion and signaling responses to collagen in a receptor density-dependent fashion. *J. Biol. Chem.* **277**, 3011–3019 (2002).
50. DeLean, A., Munson, P. J. & Rodbard, D. Simultaneous analysis of families of sigmoidal curves: application to bioassay, radioligand assay, and physiological dose-response curves. *Am. J. Physiol.* **235**, 97–102 (1978).
51. Stefanini, L. *et al.* RASA3 is a critical inhibitor of RAP1-dependent platelet activation. *J. Clin. Invest.* **125**, 1419–1432 (2015).

Acknowledgements

This research was supported by the British Heart Foundation, U.K. (grant reference: FS/13/63/30437).

Author Contributions

H.G.R., S.O.S., W.B. and G.E.J. participated in research design. H.G.R. and G.E.J. conducted the experiments. A.A.C., A.M.B., M.M. and S.M.J. contributed essential reagents and/or laboratory equipment. H.G.R. and G.E.J. performed data analysis. H.G.R. and G.E.J. wrote the manuscript.

Additional Information

Supplementary information accompanies this paper at https://doi.org/10.1038/s41598-018-34389-5.

Competing Interests: The authors declare no competing interests.

Publisher's note: Springer Nature remains neutral with regard to jurisdictional claims in published maps and institutional affiliations.